



# Temperature-dependent study of the band-edge excitonic transitions of $\text{Cu}_2\text{ZnSiS}_4$ single crystals by polarization-dependent piezoreflectance

S. Levenco<sup>a,1</sup>, D. Dumcenco<sup>a,1</sup>, Y.S. Huang<sup>a,\*</sup>, E. Arushanov<sup>b</sup>, V. Tezlevan<sup>b</sup>, K.K. Tiong<sup>c</sup>, C.H. Du<sup>d</sup>

<sup>a</sup> Department of Electronic Engineering, National Taiwan University of Science and Technology, Taipei 106, Taiwan

<sup>b</sup> Institute of Applied Physics, Academy of Sciences of Moldova, Chisinau, MD 2028, Republic of Moldova

<sup>c</sup> Department of Electrical Engineering, National Taiwan Ocean University, Keelung 202, Taiwan

<sup>d</sup> Department of Physics, Tamkang University, Tamsui 251, Taiwan

## ARTICLE INFO

### Article history:

Received 26 May 2010

Accepted 3 July 2010

Available online 14 July 2010

### PACS:

71.35.Cc

78.20.-e

78.40.Fy

### Keywords:

Semiconductors

Crystal growth

Optical properties

Optical spectroscopy

## ABSTRACT

The temperature dependence of the band-edge excitonic transitions of  $\text{Cu}_2\text{ZnSiS}_4$  single crystals were characterized by using polarization-dependent piezoreflectance (PzR) in the temperature range of 10–300 K. The PzR measurements were carried out on the as-grown basal plane with the normal along  $[2\ 1\ 0]$  and the  $c$  axis parallel to the long edge of the crystal platelet. The PzR spectra revealed polarization-dependent  $E_{\perp}^{\text{ex}}$  and  $E_{\parallel}^{\text{ex}}$  features for  $\mathbf{E}\perp\mathbf{c}$  and  $\mathbf{E}\parallel\mathbf{c}$  polarization, respectively. Both  $E_{\perp}^{\text{ex}}$  and  $E_{\parallel}^{\text{ex}}$  features are associated with the interband excitonic transitions at  $\Gamma$  point and can be explained by crystal-field splitting of valence band. From a detailed lineshape fit to the PzR spectra, the temperature dependence of the transition energies and broadening parameters of the band-edge excitons were determined accurately. The temperature dependence of near band-edge excitonic transition energies were analyzed using Varshni and Bose–Einstein expressions. The temperature dependence of the broadening parameter of excitonic features also has been studied in terms of a Bose–Einstein equation that contains the electron (exciton)–longitudinal optical phonon-coupling constant. The parameters that describe the temperature variation of the excitonic transition energies and broadening parameters were evaluated and discussed.

© 2010 Elsevier B.V. All rights reserved.

## 1. Introduction

In recent years, ternary chalcopyrites and quaternary chalcogenides have been studied to observe their semiconducting and optical properties.  $\text{Cu}_2\text{ZnSiS}_4$  is an indirect semiconductor [1] which belongs to the family of Cu-based quaternary chalcogenide compounds,  $\text{Cu}_2\text{-II-IV-VI}_4$ , crystallizing in the wurtz–stannite structure with space group  $Pmn2_1$  [2–4]. The structure of  $\text{Cu}_2\text{ZnSiS}_4$  consists of alternating cation layers of mixed Zn and Si atoms which are separated by layers of Cu atoms. It is therefore derived from an ordering of the cations of the wurtzite cell. In this compound every sulfur atom has four nearest neighbor cation atoms (two copper atoms, one zinc, and a silicon atom) at the corners of the surrounding tetrahedron [2–4]. The material is of interest for its nonlinear optical properties [5,6] and potential for application in the field of energy, environment and optoelectronics [7,8]. Despite its interesting optical properties and possible applications, up-to-date, the

theoretical and experimental understanding of the basic properties of  $\text{Cu}_2\text{ZnSiS}_4$  is still relatively incomplete [1,9], due to the difficulty of preparing high quality single crystals.

In this paper, we report a detailed study of the temperature dependence of the band-edge excitonic transitions of  $\text{Cu}_2\text{ZnSiS}_4$  single crystals by using polarization-dependent piezoreflectance (PzR) in the temperature range between 10 and 300 K. High quality single crystals of  $\text{Cu}_2\text{ZnSiS}_4$  were grown by chemical vapor transport using iodine as the transport agent. PzR has been proven to be useful in the investigation and characterization of semiconductors [10–12]. The derivative nature of PzR spectra suppresses uninteresting background effects and greatly enhances the precision in the determination of transition energies. The sharper lineshape as compared to the conventional optical techniques have enabled us to achieve a greater resolution and hence to detect weaker features. The PzR measurements were carried out on the as-grown basal plane with the normal along  $[2\ 1\ 0]$  and the axis  $c$  parallel to the long edge of the crystal platelet. The PzR spectra revealed polarization-dependent  $E_{\perp}^{\text{ex}}$  and  $E_{\parallel}^{\text{ex}}$  features for  $\mathbf{E}\perp\mathbf{c}$  and  $\mathbf{E}\parallel\mathbf{c}$  polarization, respectively. From a detailed lineshape fit, the temperature dependence of the energies and broadening parameters of the excitonic transitions near direct band-edge were determined accurately. The parameters that describe the temperature variation of

\* Corresponding author. Tel.: +886 2 27376385; fax: +886 2 27376424.

E-mail address: [ysh@mail.ntust.edu.tw](mailto:ysh@mail.ntust.edu.tw) (Y.S. Huang).

<sup>1</sup> Permanent address: Institute of Applied Physics, Academy of Science of Moldova, 5, Academiei str., MD-2028, Chisinau, Republic of Moldova.

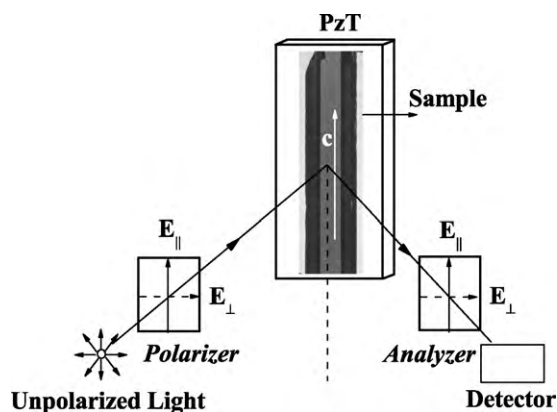


Fig. 1. A schematic arrangement of the polarization-dependent PzR measurements.

the excitonic transition energies and broadening parameter were evaluated and discussed.

## 2. Experimental

Single crystals of  $\text{Cu}_2\text{ZnSiS}_4$  were grown by vapor transport of stoichiometric amounts of the elements with 5 mg iodine/cm<sup>3</sup> as the transport agent. Optimum crystal growth was achieved with the charge zone maintained at 850 °C and the growth zone at 800 °C. The transport process was carried out for a period of 14 days. Single crystals  $\text{Cu}_2\text{ZnSiS}_4$  formed thin, greenish, blade shape up to 10 mm × 1.5 mm in area and 300 μm in thickness. The orientation of the basal plane was determined by comparing back-reflection Laue pattern with computer generated Laue plots. With the X-ray beam normal to the basal plane, the Laue pattern displayed a twofold asymmetry pattern. Analyzing the symmetry of Laue pattern confirms the formation of orthorhombic structure and reveals that the normal of the basal plane is [2 1 0] and the long edge of the crystal platelet is parallel to *c* axis. The full width at half maximum (FWHM) of the rocking curve ( $\theta$  scan) in the vicinity of (2 1 0) normal peak was determined to be  $\sim 0.007^\circ$ . The small value of FWHM indicates that high quality single crystals of  $\text{Cu}_2\text{ZnSiS}_4$  were grown.

Fig. 1 depicts the schematic arrangement of the polarization-dependent PzR measurements with polarization configurations of  $\mathbf{E}_{\perp c}$  and  $\mathbf{E}_{\parallel c}$  performed on the as-grown basal plane with the normal along [2 1 0] and *c* parallel to the long edge of the crystal platelet. A 150 W xenon arc lamp filtered by a 0.25 m grating monochromator provided the monochromatic light. Model PRH 8020 CASIX Rochon prisms were employed for polarization-dependent measurements. A model 3378 Hamamatsu photomultiplier tube was used to detect the transmitted or reflected signals. The PzR measurements were achieved by gluing the thin ( $\sim 100 \mu\text{m}$ ) single-crystal specimens on a 0.15 cm thick lead zirconate titanate piezoelectric transducer driven by a 300V<sub>rms</sub> sinusoidal wave at 200 Hz. The DC output of the reflected signal was maintained constant by a servomechanism of a variable neutral density filter. A dual-phase lock-in amplifier was used to measure the detected signals. The entire data acquisition procedure has been performed under computer control. Multiple scans over a given photon energy range was programmed until a desired signal-to-noise level has been obtained. For temperature-dependent measurements, a closed-cycle cryogenic refrigerator equipped with a digital thermometer controller was used for the low temperature measurements with a temperature stability of 0.5 K or better.

## 3. Results and discussions

Fig. 2(a) and (b) illustrates the polarization dependence of the PzR spectra of  $\text{Cu}_2\text{ZnSiS}_4$  in the vicinity of the direct band-edge at 10 and 300 K, respectively. The PzR spectra show redshifts of the transition energies and lineshape broadening characteristics as the temperature increases from 10 to 300 K. The results indicate that feature  $E_{\perp}^{\text{ex}}$  is observed in  $\mathbf{E}_{\perp c}$  polarization (open-circles) while feature  $E_{\parallel}^{\text{ex}}$  only appears in  $\mathbf{E}_{\parallel c}$  polarization (open-triangles). In order to determine the transition energies accurately, we have performed a theoretical lineshape fit. The functional form used in the fitting procedure corresponds to a first derivative Lorentzian line shape function of the form [10–13]:

$$\frac{\Delta R}{R} = \text{Re} \sum_{i=1} A_i e^{i\phi_i} (E - E_i + j\Gamma_i)^{-n} \quad (1)$$

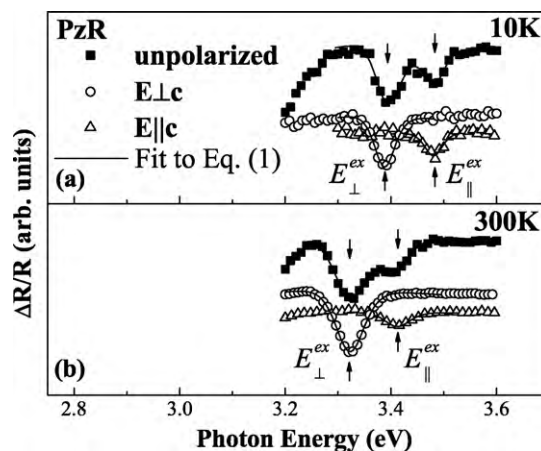


Fig. 2. The unpolarized (solid-squares),  $\mathbf{E}_{\perp c}$  polarization (open-circles) and  $\mathbf{E}_{\parallel c}$  polarization (open-triangles) PzR spectra of  $\text{Cu}_2\text{ZnSiS}_4$  at (a) 10 K and (b) 300 K. The solid lines are the least-squares fits of experimental data to Eq. (1). The obtained values of the transition energies denoted as  $E_{\perp}^{\text{ex}}$  and  $E_{\parallel}^{\text{ex}}$  are indicated by the arrows.

where  $i = \perp$  or  $\parallel$ ,  $A_i$  and  $\Phi_i$  are the amplitude and phase of the lineshape,  $E_i$  and  $\Gamma_i$  are, respectively, the energy and broadening parameter of the interband transitions. For the first derivative functional form,  $n = 2$  is appropriate for the excitonic transitions. For  $M_0$  type three-dimensional critical point interband transitions,  $n = 0.5$  is appropriate [12,13]. Our experimental signatures are more consistent with excitonic lineshape. From the spectral characteristics of the PzR spectra, the features are most probably originating from the interband excitonic transitions. Shown by the solid curves in Fig. 2(a) and (b) are the least-squares fits to Eq. (1). Arrows under the curves in Fig. 2(a) and (b) show the positions of the two interband excitonic features,  $E_{\perp}^{\text{ex}}$  and  $E_{\parallel}^{\text{ex}}$  at 10 and 300 K, respectively. The obtained values of  $E_{\perp}^{\text{ex}}$  and  $E_{\parallel}^{\text{ex}}$  at 10/300 K are  $3.389 \pm 0.003/3.323 \pm 0.005$  and  $3.482 \pm 0.003/3.413 \pm 0.005$  eV, respectively, and are listed in Table 1. The fitted values of the broadening parameters are also listed in Table 1. The unpolarized spectrum (solid-squares) can be regarded as a random superposition of the spectra with  $\mathbf{E}_{\perp c}$  and  $\mathbf{E}_{\parallel c}$  polarizations. The energy difference between the low- and high-energy transitions represents the crystal-field splitting between the two levels of the valence band and will be discussed later.

At 10 K the broadening parameters for both excitonic features are  $\sim 40$  meV and increase to  $\sim 60$  meV at 300 K. The results imply that the samples probably have many scattering centers which lead to the large values of the broadening parameters at low temperature and thereby dominate the natural intrinsic exciton linewidth which probably is much narrower. The observation of excitons at room temperature implies that the exciton binding energy is larger than 25 meV. When the temperature increases from 10 to 300 K, the broadening parameters increase by  $\sim k\Delta T$ , where  $\Delta T$  is the temperature difference. This suggests that the exciton binding energy is of order of several  $k\Delta T$ ; otherwise, the excitons would become too broad to be observed. Furthermore, the similar broadening parameter of  $\mathbf{E}_{\perp c}$  and  $\mathbf{E}_{\parallel c}$  excitonic features which is  $\sim 90$  meV apart also suggests a fairly large binding energy of  $\text{Cu}_2\text{ZnSiS}_4$ . An estimate of the exciton binding energy may be obtained using the

Table 1

Values of the excitonic transition parameters  $E_{\perp}^{\text{ex}}$ ,  $\Gamma_{\perp}$ ,  $E_{\parallel}^{\text{ex}}$  and  $\Gamma_{\parallel}$  of  $\text{Cu}_2\text{ZnSiS}_4$  obtained by fitting PzR data to Eq. (1) at 10 and 300 K.

Temperature (K)	$E_{\perp}^{\text{ex}}$ (eV)	$\Gamma_{\perp}$ (meV)	$E_{\parallel}^{\text{ex}}$ (eV)	$\Gamma_{\parallel}$ (meV)
10	$3.389 \pm 0.003$	$41 \pm 4$	$3.482 \pm 0.003$	$37 \pm 4$
300	$3.323 \pm 0.005$	$58 \pm 5$	$3.413 \pm 0.005$	$61 \pm 5$

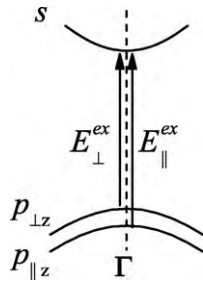


Fig. 3. A schematic representation of the plausible assignments for the observed optical transitions near direct band-edge for  $\text{Cu}_2\text{ZnSiS}_4$ .

expression for the binding energy of the ground-state exciton [14],  $E_b = -(\mu_r e^4)/2\hbar^2 \varepsilon^2$ , where  $e$  is the electron charge and  $\varepsilon$  is the dielectric constant. The index of refraction  $n$  may be deduced from an empirical relation called Moss rule where  $n^4 E_g = 77$  [15]. Take the value of  $E_g = 3.05$  eV [1], we may then evaluate  $\varepsilon \approx n^2 = 5.02$ . For a wide band gap semiconductor, a larger effective mass of electron and hole is expected [16]. Therefore, by assuming that the exciton reduced mass  $\mu_r = 0.2m_e$ , the exciton binding energy is estimated to be  $\sim 110$  meV. This result agrees well with the previous report on the orthorhombic  $\text{Cu}_2\text{Zn}_{1-x}\text{Mn}_x\text{GeS}_4$  [17]. Shih et al. reported a magnetoreflectance study of orthorhombic  $\text{Cu}_2\text{Zn}_{1-x}\text{Mn}_x\text{GeS}_4$ , where the results suggest a large exciton binding energy of the order 100 meV [17]. The experimental evidences thus far point to a general characteristic of the  $\text{Cu}_2\text{-II-IV-VI}_4$  compounds with orthorhombic structure of having a rather large exciton binding energy. A more systematic experimentation should be carried out to verify this property.

Adopting the band-structure calculation of  $\text{Cu}_2\text{ZnGeS}_4$  by Chen et al. [18], a schematic representation of the plausible assignments for the observed polarization-dependent PzR spectra of  $\text{Cu}_2\text{ZnSiS}_4$  is presented in Fig. 3. The observed near band-edge PzR spectra are attributed to the direct  $\Gamma$  point transitions from the valence band maximum (VBM) to conduction band minimum (CBM). Construction of this schematic diagram at  $\Gamma$  point is based upon two assumptions. First, the conduction and valence bands are assumed to be dominated by  $s$ -like and  $p$ -like, respectively. It is referred from the crystal structure's tetrahedral bonding arrangement which arises from  $s$ - $p^3$  hybridization. The degree of  $p$ - $d$  hybridizations is assumed to be small and can be neglected. The  $s$ -like and  $p$ -like energy bands involved in the optical transitions shall have the same symmetry properties as the atomic functions  $s$ ,  $p_{\parallel z}$  and  $p_{\perp z}$ . The second assumption is that spin-orbit splitting is much less than the crystal-filed splitting and thus may be neglected. We infer this from the PzR spectrum which exhibits one transition for  $\mathbf{E} \perp \mathbf{c}$  and a distinctly higher transition for  $\mathbf{E} \parallel \mathbf{c}$ . The energy of the transition depends strongly on the orientation of the polarization with respect to the crystallographic directions. This suggests that the orbital angular momentum of the  $p$  states is sufficiently quenched to render the spin-orbit interaction negligible. Thus the splitting between the  $\mathbf{E} \perp \mathbf{c}$  and  $\mathbf{E} \parallel \mathbf{c}$  levels of the valence band shown in Fig. 3 is attributed solely to the orthorhombic crystalline symmetry of  $\text{Cu}_2\text{ZnSiS}_4$  which is described by the space group  $Pmn2_1$ .

The temperature-dependent PzR spectra of  $\text{Cu}_2\text{ZnSiS}_4$  with  $\mathbf{E} \perp \mathbf{c}$  and  $\mathbf{E} \parallel \mathbf{c}$  polarizations at 10, 77, 150, 225 and 300 K are shown in Fig. 4. The open-circles and triangles curves are, respectively, the experimental PzR spectra of  $\mathbf{E} \perp \mathbf{c}$  and  $\mathbf{E} \parallel \mathbf{c}$  polarizations, while the solid curves are the least-squares fits to Eq. (1). Arrows below the curves in Fig. 4 show the positions of the two interband excitonic features. As the general property of most semiconductors, the excitonic transitions in the PzR spectra exhibit a redshift and lineshape broadening when the temperature is increased.

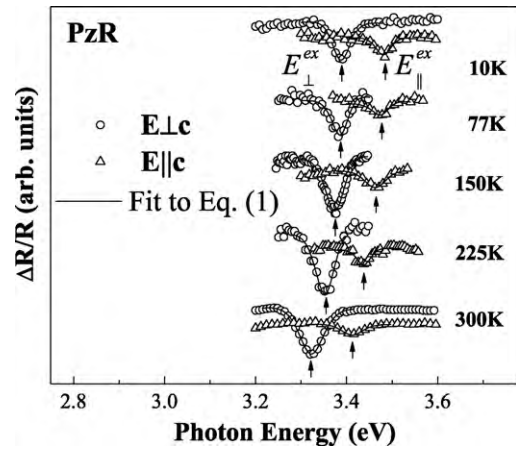


Fig. 4. The  $\mathbf{E} \perp \mathbf{c}$  polarization (open-circles) and  $\mathbf{E} \parallel \mathbf{c}$  polarization (open-triangles) PzR spectra of  $\text{Cu}_2\text{ZnSiS}_4$  at 10, 77, 150, 225 and 300 K. The solid lines are the least-squares fits of experimental data to Eq. (1). The obtained transition energies are denoted by arrows.

Fig. 5 shows the fitted data of temperature dependence of the  $E_{\perp}^{\text{ex}}$  and  $E_{\parallel}^{\text{ex}}$  excitonic transition energies. The uncertainties in experimental data are expressed in the form of the representative error bars. The solid curves in Fig. 4 are the least-squares fits to the Varshni empirical relationship [19]:

$$E^{\text{ex}}(T) = E_i(0) - \frac{\alpha_i T^2}{\beta_i + T}, \quad (2)$$

where  $i = \perp$  or  $\parallel$ ,  $E_i(0)$  is the excitonic transition energy at 0 K, and  $\alpha_i$  and  $\beta_i$  are the Varshni coefficients. The constant  $\alpha_i$  is related to the electron (exciton)–phonon interaction and  $\beta_i$  is closely related to the Debye temperature. The obtained values of  $E_i(0)$ ,  $\alpha_i$  and  $\beta_i$  corresponding to the excitonic transitions for  $\text{Cu}_2\text{ZnSiS}_4$  are listed in Table 2. For comparison purposes the numbers from previous reports on freestanding wurtzite WZ-GaN [20], GaAs [21], ZB-ZnSe [22] and ZB-ZnS [23] are listed in Table 2.

The temperature dependence of the interband excitonic transition energies  $E_{\perp}^{\text{ex}}$  and  $E_{\parallel}^{\text{ex}}$  can also be fitted (dashed curve) by an expression containing the Bose–Einstein occupation factor for phonon [21,24]:

$$E^{\text{ex}}(T) = E_i(0) - \frac{2a_{Bi}}{[\exp(\Theta_{Bi}/T) - 1]}, \quad (3)$$

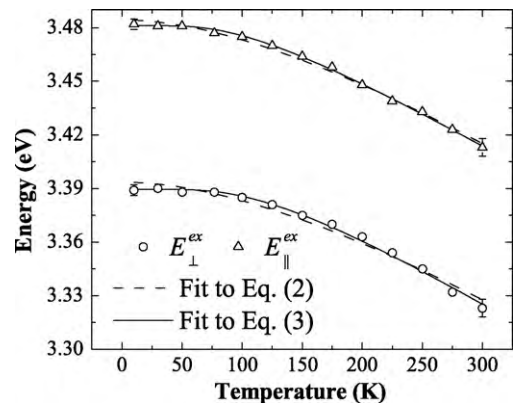


Fig. 5. Dependence on temperature of the excitonic transition energies of  $\text{Cu}_2\text{ZnSiS}_4$ . The open-circles and triangles are energies of the  $E_{\perp}^{\text{ex}}$  and  $E_{\parallel}^{\text{ex}}$  excitonic transitions, respectively, with representative error bars. The dashed and solid curves represent the fit to the Varshni (Eq. (2)) and Bose–Einstein (Eq. (3)) expressions, respectively.

**Table 2**

Values of the Varshni and Bose Einstein parameters of  $\text{Cu}_2\text{ZnSiS}_4$  obtained by fitting the temperature dependence data of the  $E_{\perp}^{\text{ex}}$  and  $E_{\parallel}^{\text{ex}}$  excitonic transition energies to Eqs. (2) and (3), respectively. The corresponding values for the freestanding WZ-GaN, GaAs, ZB-ZnSe and ZB-ZnS are also listed for comparison.

Materials	Feature	$E(0)$ (eV)	$\alpha$ ( $10^{-4}$ eV/K)	$\beta$ (K)	$a_B$ (meV)	$\Theta_B$ (K)
$\text{Cu}_2\text{ZnSiS}_4$	$E_{\perp}^{\text{ex}}$	$3.390 \pm 0.003$	$5 \pm 1$	$380 \pm 90$	$80 \pm 10$	$370 \pm 50$
	$E_{\parallel}^{\text{ex}}$	$3.482 \pm 0.003$	$5 \pm 1$	$350 \pm 100$	$70 \pm 10$	$340 \pm 50$
WZ-GaN <sup>a</sup>	$A^{\text{ex}}$	$3.490 \pm 0.001$	$10.4 \pm 0.8$	$1100 \pm 100$	$75 \pm 20$	$350 \pm 50$
	$B^{\text{ex}}$	$3.500 \pm 0.001$	$10.5 \pm 0.8$	$1100 \pm 100$	$75 \pm 20$	$350 \pm 50$
	$C^{\text{ex}}$	$3.520 \pm 0.001$	$10.6 \pm 0.8$	$1100 \pm 100$	$76 \pm 20$	$350 \pm 50$
GaAs <sup>b</sup>	$E_g$	$1.517 \pm 0.008$	$5.5 \pm 1.3$	$225 \pm 174$	$57 \pm 29$	$240 \pm 50$
ZB-ZnSe <sup>c</sup>	$E_g$	$2.800 \pm 0.005$	$7.3 \pm 1$	$295 \pm 35$	$73 \pm 4$	$260 \pm 10$
ZB-ZnS <sup>d</sup>	$E_g$	3.844	6.3	250	73	272

<sup>a</sup> Ref. [20].

<sup>b</sup> Ref. [21].

<sup>c</sup> Ref. [22].

<sup>d</sup> Ref. [23].

where  $i = \perp$  or  $\parallel$ ,  $E_i(0)$  is the excitonic transition energy at 0 K,  $a_{Bi}$  represents the strength of the electron (exciton)–phonon interaction, and  $\Theta_{Bi}$  corresponds to the average phonon temperature. The fitted values for  $E_i(0)$ ,  $a_{Bi}$ , and  $\Theta_{Bi}$  are given in Table 2, and the corresponding values for freestanding WZ-GaN [20], GaAs [21], ZB-ZnSe [22] and ZB-ZnS [23] are also listed in Table 2 for comparison.

The parameter  $\alpha_i$  in Eq. (2) can be related to  $a_{Bi}$  and  $\Theta_{Bi}$  in Eq. (3) by taking the high-temperature limit of both expressions, which yields to  $\alpha_i = 2a_{Bi}/\Theta_{Bi}$ . Comparison of the values presented in Table 2 shows that this relation is indeed satisfied. From Eq. (3) it is straightforward to show that the high-temperature limit of the slope of  $E^{\text{ex}}(T)$  versus  $T$  curve approaches the value of  $-2a_{Bi}/\Theta_{Bi}$ . The calculated values of  $-2a_{Bi}/\Theta_{Bi}$  for  $E_{\perp}^{\text{ex}}$  and  $E_{\parallel}^{\text{ex}}$  equal to  $-0.43$  and  $-0.41$  meV/K for  $\mathbf{E}_{\perp}\mathbf{c}$  and  $\mathbf{E}_{\parallel}\mathbf{c}$ , respectively, which agree well with the values of  $dE_{\perp}^{\text{ex}}/dT = -0.41$  meV/K and  $dE_{\parallel}^{\text{ex}}/dT = -0.37$  meV/K obtained from linear extrapolation in the higher temperature (200–300 K) PzR experimental data.

The fitted values of the broadening parameters of the  $E_{\perp}^{\text{ex}}$  and  $E_{\parallel}^{\text{ex}}$  features for  $\text{Cu}_2\text{ZnSiS}_4$  with representative error bars are displayed in Fig. 6. The temperature dependence of the broadening parameters of semiconductors can be expressed as [21]:

$$\Gamma_i(T) = \Gamma_{i0} + \frac{\Gamma_{iLO}}{[\exp(\Theta_{iLO}/T) - 1]}, \quad (4)$$

where  $i = \perp$  or  $\parallel$ , the first term of Eq. (4) represents the broadening invoked from temperature-independent mechanisms, such as electron–electron interactions, impurity or dislocation, whereas the second term is caused by the electron (exciton)–longitudinal optical (LO) phonon (Fröhlich) interaction. The quantity  $\Gamma_{iLO}$  rep-

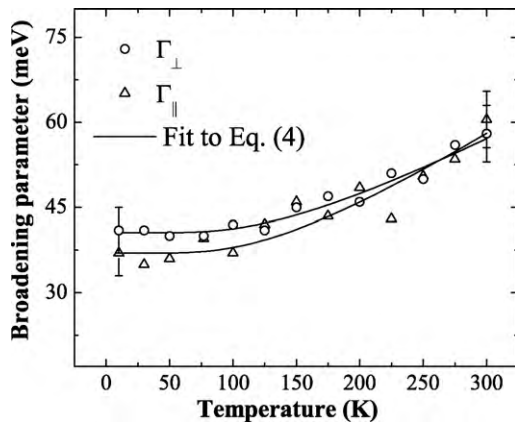


**Fig. 6.** Temperature-dependent broadening parameters of the excitonic features of  $\text{Cu}_2\text{ZnSiS}_4$ . The open-circles and triangles are broadening parameters of the  $E_{\perp}^{\text{ex}}$  and  $E_{\parallel}^{\text{ex}}$  features, respectively, with representative error bars. The solid curves represent the least-squares fits of the data to Eq. (4).

**Table 3**

Values of the  $\Gamma_0$ ,  $\Gamma_{LO}$  and  $\Theta_{LO}$  parameters of  $\text{Cu}_2\text{ZnSiS}_4$  obtained by fitting the temperature dependence of the broadening parameters of the  $E_{\perp}^{\text{ex}}$  and  $E_{\parallel}^{\text{ex}}$  features to Eq. (4). For comparison the numbers for GaAs and ZB-ZnSe are listed.

Materials	Feature	$\Gamma_0$ (meV)	$\Gamma_{LO}$ (meV)	$\Theta_{LO}$ (K)
$\text{Cu}_2\text{ZnSiS}_4$	$E_{\perp}^{\text{ex}}$	$41 \pm 5$	$55 \pm 12$	$440 \pm 90$
	$E_{\parallel}^{\text{ex}}$	$37 \pm 5$	$65 \pm 15$	$420 \pm 120$
GaAs <sup>a</sup>	$E_g$	2	$20 \pm 1$	417
ZB-ZnSe <sup>b</sup>	$E_g$	$6.5 \pm 2.5$	$24 \pm 8$	360

<sup>a</sup> Ref. [25].

<sup>b</sup> Ref. [22].

resents the strength of the electron (exciton)–LO phonon coupling while  $\Theta_{iLO}$  is the LO phonon temperature [21]. The solid curves in Fig. 6 are least-squares fits to Eq. (4), which made it possible to evaluate  $\Gamma_{i0}$ ,  $\Gamma_{iLO}$  and  $\Theta_{iLO}$  for the excitonic transitions of  $\text{Cu}_2\text{ZnSiS}_4$ . The obtained values of these quantities are listed in Table 3 together with the numbers for GaAs [25], and ZB-ZnSe [22].

As listed in Table 3, the values of  $\Gamma_{\perp 0}$  and  $\Gamma_{\parallel 0}$  for the excitonic transitions are determined to be approximately 41 and 37 meV, respectively. The large values of  $\Gamma_{i0}$  imply that the sample probably have many scattering centers such as compositional fluctuations, alloy scattering, electron–electron interaction, impurity and dislocation etc. From Tables 2 and 3, it can be seen that  $\Theta_{iLO}$  is higher than  $\Theta_{iB}$ . The smaller values  $\Theta_{iB}$  to the relevant to  $\Theta_{iLO}$  can be caused by the contribution of the acoustic and optical phonons to the temperature variation of the excitonic gap energy whereby  $\Theta_{iLO}$  is due to the electron (exciton)–LO phonon coupling [21,24]. The values for the exciton–LO phonon-coupling parameters,  $\Gamma_{\perp LO}$  and  $\Gamma_{\parallel LO}$ , obtained by the fit to Eq. (4) are 55 and 65 meV, respectively, which are considerably larger than those reported for GaAs (20 meV) [25] and ZnSe (24 meV) [22]. The larger value of  $\Gamma_{LO}$  might be due to the much larger average LO phonon in comparison to that of ZnSe and GaAs. In addition, it is possible that a larger deformation potential interaction, which may account for a significant fraction of  $\Gamma_{LO}$  in addition to the Fröhlich interaction, is responsible for the larger  $\Gamma_{LO}$ .

#### 4. Summary

The temperature dependence of the band-edge excitonic transitions of  $\text{Cu}_2\text{ZnSiS}_4$  single crystals were characterized by using polarization-dependent PzR in the temperature range between of 10 and 300 K. The single crystals of  $\text{Cu}_2\text{ZnSiS}_4$  were grown by chemical vapor transport technique using iodine as transport agent. The PzR measurements were carried out on the as-grown basal plane with the normal along [210] and the  $\mathbf{c}$  axis parallel to the long edge of the crystal platelet. The PzR spectra revealed polarization-dependent  $E_{\perp}^{\text{ex}}$  and  $E_{\parallel}^{\text{ex}}$  features for  $\mathbf{E}_{\perp}\mathbf{c}$  and  $\mathbf{E}_{\parallel}\mathbf{c}$  polar-

ization, respectively. The splitting of 90 meV between the  $E_{\perp c}$  and  $E_{\parallel c}$  levels at the  $\Gamma$  point of the valence band may be attributed solely to the orthorhombic crystalline symmetry of  $\text{Cu}_2\text{ZnSi}_4$  which is described by the space group  $Pmn2_1$ . From a detailed line-shape fit to the PzR spectra, the temperature dependence of the transition energies and broadening parameters of the band-edge excitons were determined accurately. The temperature dependence of the near band-edge excitonic transition energies has been analyzed by both Varshni- and Bose–Einstein-type expressions. The parameters extracted from both expressions by extending into the high-temperature regime are found to agree reasonably well. The parameters that describe the temperature dependence of the broadening function of the band-edge excitonic features have also been studied. The electron (exciton)– $LO$  phonon-coupling constant,  $\Gamma_{LO}$ , are determined to be considerably larger than that reported for GaAs and ZnSe. The larger value of  $\Gamma_{LO}$  might be due to the much larger average  $LO$  phonon in comparison to that of ZnSe and GaAs. In addition, it is possible that a larger deformation potential interaction, which may account for a significant fraction of  $\Gamma_{LO}$  in addition to the Fröhlich interaction, is responsible for the larger  $\Gamma_{LO}$ .

### Acknowledgments

The authors acknowledge the support of National Science Council of Taiwan under Project Nos. NSC 098-2811-E-011-019, NSC 97-2112-M-011-001-MY3 and 98-2221-E-011-015-MY2.

### References

- [1] G.Q. Yao, H.S. Shen, E.D. Honig, R. Kershaw, K. Dwight, A. Wold, *Solid State Ionics* 24 (1987) 249–252.
- [2] R. Nitsche, D.F. Sargent, P. Wild, *J. Cryst. Growth* 1 (1967) 52–53.
- [3] W. Schafer, R. Nitsche, *Mater. Res. Bull.* 9 (1974) 645–654.
- [4] L. Guen, M.S. Glasinger, A. Wold, *Mater. Res. Bull.* 14 (1979) 463–467.
- [5] J.W. Lekse, M.A. Moreau, K.L. McNerny, J. Yeon, P.S. Halasyamani, J.A. Aitken, *Inorg. Chem.* 48 (2009) 7516–7518.
- [6] J.W. Lekse, B.M. Leverett, C.H. Lake, J.A. Aitken, *J. Solid State Chem.* 181 (2008) 3217–3222.
- [7] H. Matsushita, A. Katsui, *J. Phys. Chem. Solids* 66 (2005) 1933–1936.
- [8] T. Oike, T. Iwasaki, 2000, AH01L2915FI, <http://www.faq.org/patents/app/20080303035#ixzz0iW8PX6KV>.
- [9] D.M. Schleich, A. Wold, *Mater. Res. Bull.* 12 (1977) 111–114.
- [10] F.H. Pollak, H. Shen, *Mater. Sci. Eng. R* 10 (1993) xv–xvi.
- [11] H. Mathieu, J. Allegre, B. Gil, *Phys. Rev. B* 43 (1991) 2218–2227.
- [12] Y.S. Huang, F.H. Pollak, *Phys. Status Solidi A* 202 (2005) 1193–1207.
- [13] D.E. Aspnes, in: T.S. Moss, M. Balkanski (Eds.), *Handbook of Semiconductors*, vol. 2, North-Holland, Amsterdam, 1980, pp. 109–154.
- [14] D.L. Dexter, R.S. Knox, *Excitons*, Interscience, New York, 1965, p. 53.
- [15] T.S. Moss, *Optical Properties of Semiconductors*, Butterworths, London, 1959, p. 48.
- [16] C.J. Nuese, in: W. Bardsley, D.T.J. Hurle, J.B. Mullin (Eds.), *Crystal Growth: A Tutorial Approach*, North-Holland, Amsterdam, 1979, p. 358.
- [17] O.W. Shih, R.L. Aggarwal, T.Q. Vu, Y. Shapira, K. Doverspike, R.N. Kershaw, K. Dwight, A. Wold, *Phys. Rev. B* 45 (1992) 14025–14035.
- [18] S. Chen, X.G. Gong, A. Walsh, S.H. Wei, *Phys. Rev. B* 79 (2009) 165211.
- [19] Y.P. Varshni, *Physica (Utrecht)* 34 (1967) 149–154.
- [20] Y.S. Huang, F.H. Pollak, S.S. Park, K.Y. Lee, H. Morkos, *J. Appl. Phys.* 94 (2003) 899–903.
- [21] P. Lautenschlager, M. Garriga, S. Logothetidis, M. Cardona, *Phys. Rev. B* 35 (1987) 9174–9189.
- [22] L. Malikova, W. Krystek, F.H. Pollak, N. Dai, A. Cavus, M.C. Tamargo, *Phys. Rev. B* 54 (1996) 1819–1824.
- [23] R. Passler, E. Griebel, H. Riepl, G. Lautner, S. Bauer, H. Preis, W. Gebhardt, B. Buda, D.J. As, D. Schikora, K. Lischka, K. Papagelis, S. Ves, *J. Appl. Phys.* 86 (1999) 4403–4411.
- [24] P. Lautenschlager, M. Garriga, L. Vina, M. Cardona, *Phys. Rev. B* 36 (1987) 4821–4830.
- [25] H. Qiang, F.H. Pollak, C.M. Sotomayor Torres, W. Leitch, A.H. Kean, M. Stroscio, G.J. Jafraite, K.W. Kim, *Appl. Phys. Lett.* 61 (1992) 1411–1413.